Nanoscale Res Lett (2008) 3:508–515
DOI 10.1007/s11671-008-9188-3

NANO EXPRESS

Fabrication and Properties of Ethylene Vinyl Acetate-Carbon Nanofiber Nanocomposites

Jinu Jacob George · Anil K. Bhowmick

Received: 29 June 2008 / Accepted: 3 October 2008 / Published online: 25 October 2008

Abstract Carbon nanofiber (CNF) is one of the stiffest materials produced commercially, having excellent mechanical, electrical, and thermal properties. The reinforcement of rubbery matrices by CNFs was studied in the case of ethylene vinyl acetate (EVA). The tensile strength was greatly (61%) increased, even for very low fiber content (i.e., 1.0 wt.%). The surface modification of the fiber by high energy electron beam and gamma irradiation led to better dispersion in the rubber matrix. This in turn gave rise to further improvements in mechanical and dynamic mechanical properties of EVA. The thermal conductivity also exhibited improvements from that of the neat elastomer, although thermal stability of the nanocomposites was not significantly altered by the functionalization of CNFs. Various results were well supported by the morphological analysis of the nanocomposites.

Keywords Nanocomposite · Carbon nanofiber · EVA · Reinforcement · Elastomers

Introduction

Carbon nanofibers (CNFs) that are much smaller than conventional carbon fibers but significantly larger than carbon nanotubes (CNTs) can be used to produce nanocomposites with excellent properties, which may open up many new applications. They are available in diameters ranging from 70 and 200 nm and length estimated to be 50–100 μm [1, 2]. CNFs generally exhibit a bamboo-like conical structure as observed in transmission electron micrographs (TEM) (J.J. George and A.K. Bhowmick, personal communication).

Use of CNFs as reinforcement to improve properties of various polymer matrix systems like polycarbonate, epoxy, polyethylene, polypropylene, polymethyl methacrylate, polyether ether ketone, and polystyrene has already been demonstrated [3–20]. The results show enhancement in mechanical [7–10, 19], thermal [7–9], and dielectric/electrical [12–17] properties. The key technical challenges which remain for such nanofiber-reinforced polymers are the achievement of a homogeneous dispersion and good interfacial bonding. The smaller diameter and greater surface area of the nanofibers also imply stronger interactions among the nanofibers; hence, it is often difficult to disperse them into a polymer matrix. Thus, if the dispersion of the nanofibers is less than ideal, it impairs the resultant nanocomposite properties. Making composites with optimal properties requires adequate fiber-matrix adhesion, which is governed by the chemical and physical interactions occurring at the interface. If the fiber to matrix adhesion is poor, a composite may fail at the interface, reducing in particular the tensile strength.

In this article, elastomer grade ethylene vinyl acetate (EVA) having 50% vinyl acetate (VA) content has been chosen as the base matrix. The properties of the composites formed with as-received CNFs and various treated nanofibers are compared, with the idea that the modified CNFs contain surface defect sites and surface polar groups, which can form intermolecular interactions with the polar molecules in the matrix polymer. The presence of such defect sites and surface groups on the pristine CNFs is limited. The quality of the nanofiber dispersion in the polymer matrix is observed by TEM and is then correlated with the mechanical, dynamic mechanical, and thermal properties to

J. J. George · A. K. Bhowmick (✉)
Rubber Technology Centre, Indian Institute of Technology, Kharagpur 721302, India
e-mail: anilkb@rtc.iitkgp.ernet.in

provide insight into the role of the CNF surface modification and interfacial interactions on the ultimate properties of the resultant nanocomposites. In our earlier communications, we have shown that appropriate modifications of graphite and multiwalled CNTs can enhance the physico mechanical properties of the nanocomposites [21, 22].

Experimental

Materials

CNFs (as-grown grade PR-24 AG Pyrograf—IIITM) were obtained from Applied Sciences Inc., USA. The CNF consists of a mixture of two distinctive structures present in the sample, relatively straight cylindrical tubes and the so-called bamboo tube-like structures, arranged into loose aggregates. The diameter of CNFs varied between 70 and 200 nm and length between 50 and 100 μm. CNFs used had an aspect ratio (length-to-diameter) of over 500 in the as-received state and is free of carbonaceous contamination. High-resolution TEM micrograph of the surface of CNF shows stacking of graphene layers, distance between graphitic planes being 0.334 nm.

EVA elastomer with 50% VA content was supplied by Bayer (now Lanxess), Germany. The cross-linker for the rubber phase, dicumyl peroxide (DCP, 99% pure), was obtained from Hercules India. Triallyl cyanurate (TAC), the co-agent, was procured from Fluka A G, Germany. Tetrahydrofuran (THF) of LR grade, used as the solvent for EVA, was obtained from MERCK (India) Ltd., Mumbai, India.

Surface Treatment with High-energy Radiations

Electron Beam Irradiation

The CNFs were irradiated by electron beam (EB) accelerator (model ILU-6) at BARC, Mumbai, India. Irradiation doses used were 50, 200, and 800 kGy (dose per pass was fixed at 10 kGy) at room temperature. A FWT-60 dosimeter based on calibration obtained from gamma-radiation was used for the EB dosimetry. The accelerator voltage frequency was 100–120 MHz and the energy range was 0.5–2.0 MeV.

Gamma Irradiation

The CNF samples were irradiated with gamma rays at three different doses −1, 5, and 10 kGy, using GC 5000 (Source: Co-60) at a dose rate of 3.2 kGy/h. This was carried out at the gamma irradiation facility in BARC, Mumbai, India.

Chemical Modifications

Amine Treatment

The amination of CNFs was done by treating 200 mg of the sample with excess of hexamethylene diamine within a 50-mL thick-walled test tube at 130 ± 10 °C in an oil bath for 24 h. The treated sample was then washed with alcohol to remove the excess amine followed by washing with distilled water to remove the alcohol present. The nanofibers were then filtered using nylon membrane filter paper of 0.45-μm pore size. It was then dried in vacuum oven at 80 °C for 4 h.

Acid Treatment

CNFs (200 mg) were sonicated with H_2SO_4/HNO_3 mixture (3:1) for 3 h at 40 °C. The treated samples were washed with distilled water repeatedly until the pH of the mixture came to 6. The nanofibers were then filtered using nylon membrane filter paper of 0.45-μm pore size. These were then dried in vacuum oven at 80 °C for 4 h.

Silane Treatment

CNFs were functionalized via refluxing with 1 g of vinyl-silane in 25-mL of THF at 80 °C for 8 h. The free radical reaction was initiated by benzoyl peroxide (0.1 g) added to the mixture. Modified nanofibers were washed several times with anhydrous THF.

Table 1 Sample designations

Sample designation	Description
CNF	Untreated carbon nanofiber
$CNF_{EB\text{-}800\ kGy}$	CNF-treated with 800 kGy EB
$CNF_{\gamma\text{-}1\ kGy}$	CNF-treated with 1 kGy Gamma irradiation
ACNF	Amine-treated carbon nanofiber
XCNF	Acid-treated carbon nanofiber
SCNF	Silane-treated carbon nanofiber
EVA	Neat elastomer
EVA-1F	EVA filled with 1 wt.% of untreated CNF
EVA-4F	EVA filled with 4 wt.% of untreated CNF
EVA-8F	EVA filled with 8 wt.% of untreated CNF
$EVA\text{-}1F_{EB}$	EVA filled with 1 wt.% of 800 kGy EB irradiated CNF
$EVA\text{-}1F_{\gamma}$	EVA filled with 1 wt.% of 1 kGy Gamma irradiated CNF
EVA-1AF	EVA filled with 1 wt.% of amine treated CNF
EVA-1XF	EVA filled with 1 wt.% of acid treated CNF
EVA-1SF	EVA filled with 1 wt.% of silane treated CNF

All the treated and untreated CNFs were analyzed using different morphological, elemental, structural, and thermal characterization techniques. The detailed results of various characterizations were provided elsewhere (J.J. George and A.K. Bhowmick, personal communication).

The sample designations are given in Table 1.

Preparation of EVA-CNF Nanocomposites

The nanocomposites were synthesized by using a solution-mixing technique. EVA (5 g per batch) was dissolved in 50-mL of THF to make 10% solution of the rubber using a mechanical stirrer. 0.05 g of DCP as the curing agent and 0.05 g of TAC as the co-agent were added to the rubber solution. The solution was thoroughly stirred using a mechanical stirrer. CNFs dispersed in THF were first sonicated for 15 min and subsequently added to the rubber solution while stirring at room temperature (27 °C). The final solution was cast over Teflon trays and kept for air drying followed by vacuum drying at 50 °C till there was practically no weight variation. The dried films were molded in a hot press at a pressure of 5 MPa at 150 °C for an optimum cure time of 25 min, determined from a Monsanto oscillating disc rheometer (100S).

Morphological Study

The microscopy was performed using a JEOL JEM-2010 (Japan), TEM operating at an accelerating voltage of 200 kV. The composite samples were cut by ultra-cryo-microtomy using a Leica Ultracut UCT. Freshly sharpened glass knives with cutting edge of 45° were used to get the cryosections of 50–70 nm thickness. Since these samples were elastomeric in nature, the temperature during ultra-cryomicrotomy was kept at −50 °C (which was well below the glass transition temperature of EVA). The cryosections were collected individually on sucrose solution and directly supported on a copper grid of 300-mesh size.

Morphological comparison of untreated and acid-treated CNFs was performed using an SEM model JSM800 manufactured by JEOL at 20 kV acceleration voltage at room temperature.

Mechanical and Dynamic Mechanical Analysis

The mechanical properties of the nanocomposites were evaluated by a universal testing machine (Zwick 1445) on dumbbell specimens, punched out from the cast films using an ASTM Die C. All the tests were carried out as per ASTM D 412-99 method at 25 ± 2 °C at a crosshead speed of 500 mm/min. The average values of three tests for tensile strength, tensile modulus, and elongation at break are reported for each sample.

Dynamic mechanical thermal characteristics of the composite films (0.4–0.6-mm thick) were evaluated by using a DMTA IV (Rheometric Scientific) under tension mode. All the data were analyzed using RSI Orchestrator application software on an ACER computer attached to the machine. The temperature sweep measurements were made from −35 to 20 °C. The experiments were carried out at a frequency of 1 Hz at a heating rate of 2 °C/min. The strain amplitude used in the DMA test was 0.01% and the soak time at −35 °C was 3 min. The storage modulus (E') and the loss tangent (tan δ) data were recorded for all the samples under identical conditions.

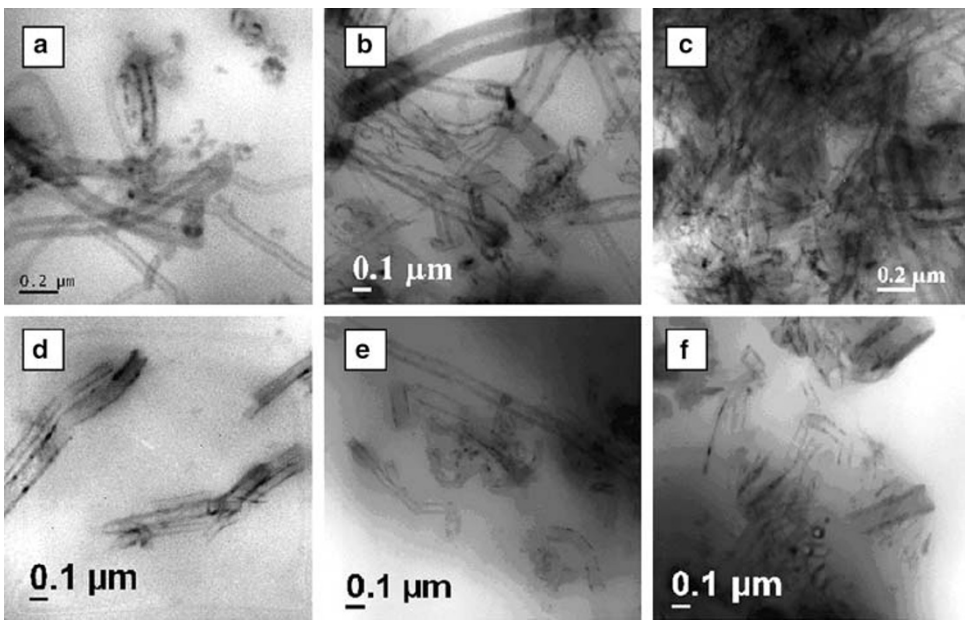

Fig. 1 TEM micrographs of representative nanocomposites **a** EVA-1F, **b** EVA-4F, **c** EVA-8F, **d** EVA-1F$_{EB}$, **e** EVA-1F$_{\gamma}$, and **f** EVA-1SF

Swelling Analysis

The swelling studies of the rubber specimens were carried out in toluene at ambient conditions (27 °C) for 72 h. Volume fraction of rubber, V_r, was calculated using the following equation [20]

$$V_r = \frac{(D - FT)\rho_r^{-1}}{(D - FT)\rho_r^{-1} + A_0\rho_s^{-1}}, \quad (1)$$

where, V_r is the volume fraction of rubber in the swollen gel, D the de-swollen weight of the composites, F the fraction insoluble, T the initial weight of the sample, and A_0 the amount of solvent imbibed. ρ_r is the density of the rubber, while ρ_s is density of the swelling solvent.

Thermal Conductivity

The thermal conductivity of the various nanocomposites was measured as per ASTM C177. The thermal conductivity was calculated using the equation

$$K = \frac{Wt}{A\ \mathrm{d}T}, \quad (2)$$

where W is the power in Watts (here 4 W), K the thermal conductivity, t the thickness of sample, A the area of the sample, and dT the temperature difference between the two plates.

Thermal Degradation Studies

Thermal stability of the composites was investigated by thermo gravimetric analysis (TGA) by using a Perkin–Elmer TGA instrument (Model: Pyris Diamond TG/DTA) from ambient to 800 °C at a programed heating rate of 20 °C/min in nitrogen. A sample weight of approximately 10 mg was taken for all the measurements. The weight loss against temperature was recorded. Differential thermo gravimetric analysis (DTG) of the composites was represented in terms of the first derivative plots of the TGA curves. The data points denote the weight loss/time against temperature at the specified heating rate.

Results and Discussion

Morphological Study by TEM

Figure 1a–f displays the TEM photographs of EVA-1F, EVA-4F, EVA-8F, EVA-1F$_{EB}$, EVA-1F$_{\gamma}$, and EVA-1SF. It can be seen that the CNFs are well dispersed in the EVA matrix up to 4 wt.% loading although there is presence of a few agglomerates. However, at a higher loading of 8 wt.%, the agglomerations start dominating, as evident from

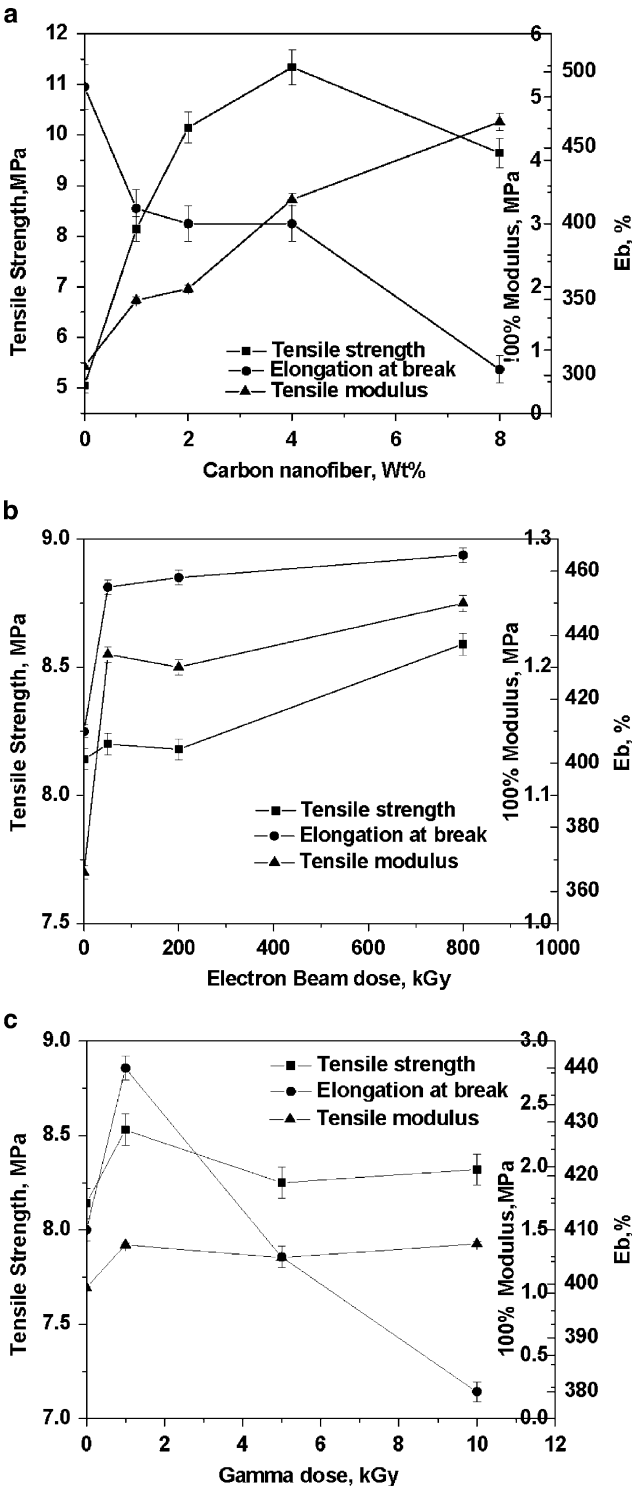

Fig. 2 **a** Effect of filler loading on the mechanical properties of nanocomposites. **b** Effect of EB irradiation dose on the mechanical properties of nanocomposites. **c** Effect of gamma irradiation dose on the mechanical properties of nanocomposites

Fig. 1c. Various modified CNF filled nanocomposites exhibit better dispersion of the nanofibers. This can be due to the improved filler–polymer interaction developed

Table 2 Tensile properties of various nanocomposites

Sample	Tensile strength (MPa)	Elongation at break (%)	Modulus at 100% elongation (MPa)
EVA	5.05 ± 0.15	490 ± 30	0.74 ± 0.17
EVA-1F	8.14 ± 0.20	410 ± 20	1.04 ± 0.21
EVA-1F$_{EB}$	8.53 ± 0.11	465 ± 20	1.25 ± 0.12
EVA-1F$_{\gamma}$	8.60 ± 0.15	440 ± 15	1.38 ± 0.15
EVA-1AF	8.25 ± 0.12	432 ± 25	1.30 ± 0.10
EVA-1XF	6.86 ± 0.18	323 ± 30	1.02 ± 0.16
EVA-1SF	8.50 ± 0.10	436 ± 15	1.36 ± 0.14

because of the presence of polar groups covalently attached on the fiber surfaces in addition to generation of surface defects. The amount of defects on CNFs has been estimated by calculating the I_D/I_G intensity ratio from the Raman spectra, where, I_D and I_G are the intensities of well-known D and G band peaks of carbon materials, respectively (J.J. George and A.K. Bhowmick, personal communication). The ratio between the disorder and the order transition (I_D/I_G) gives the information about the generation of surface defects due to functionalization. I_D/I_G value of untreated CNF is 0.64. The various modified samples CNF$_{EB\text{-}800\ kGy}$, CNF$_{\gamma\text{-}1\ kGy}$, ACNF, XCNF, and SCNF have I_D/I_G values of 0.77, 0.78, 0.70, 0.84, and 0.68, respectively. This shows that after various modifications, the amount of surface defects has increased. The presence of surface defects increases the effective surface area of nanofibers and hence their interaction with polymer chains. The relative concentration of oxygen, attached to C=O group increases by 5.5% from 28.9 (untreated) to 30.5% after EB irradiation and increases by 13.1% from 28.9 to 32.7% after gamma irradiation. Similarly, ACNF and SCNF exhibit presence of respective polar functional groups (J.J. George and A.K. Bhowmick, personal communication).

Mechanical and Dynamic Mechanical Analysis

Plotted in Fig. 2a is the variation of tensile properties of EVA with the incorporation of different amounts of untreated CNF. The tensile strength exhibits a continuous increment up to 4 wt.% CNF loading, indicating finer fiber–polymer interaction up to that level (confirmed from swelling experiments). An improvement of tensile strength of 61 and 125% is observed after the addition of 1 and 4 wt.% of CNFs, respectively. Further addition of CNF (8 wt.%) exhibits a decline in tensile strength due to poor dispersion and agglomeration of filler particles, as observed in TEM photograph. The addition of CNF imparts improvement in tensile modulus as well, as expected from the addition of any filler. The modulus exhibits a tremendous increment of 350 and 520% with the addition of 4 and 8 wt.% of CNF, respectively. The elongation at break, on the other hand, shows steep decrement with the amount of CNF.

The effects of various high-energy treatments of CNFs on the tensile properties of EVA nanocomposites are displayed in Fig. 2b and c. All the tensile properties show increment with EB dose up to 800 kGy. On the other hand, gamma irradiation of 1 kGy provides best tensile properties, beyond which there is no significant improvement. In Table 2, the tensile properties of EB, gamma, and various chemically treated CNF-reinforced nanocomposites are also compared with those of virgin EVA and untreated CNF-reinforced nanocomposite at 1 wt.% loading. Maximum improvement in tensile modulus occurs for the samples EVA-1F$_{\gamma}$ and EVA-1SF. The increments are 33 and 31% over the untreated CNF-filled composite, while the samples EVA-1F$_{EB}$ and EVA-1AF display increments of 20 and 25%, respectively (Table 2). The acid treatment adversely affected the nanocomposite tensile properties (cf. EVA-1XF). This may be due to the degradation undergone by the CNF upon acid treatment. The decrease in tensile properties of XCNF-filled samples are due to the breakage of the nanofibers. This is evident from the SEM pictures displayed in Fig. 3a and b.

The tan δ and storage modulus (inset) of the various nanocomposites with 1, 4, and 8 wt.% untreated CNFs and 1 wt.% treated CNFs are plotted as a function of temperature in Fig. 4a–c. At −30.8 °C (T_g of EVA), a modest enhancement of 5% in the storage modulus is observed

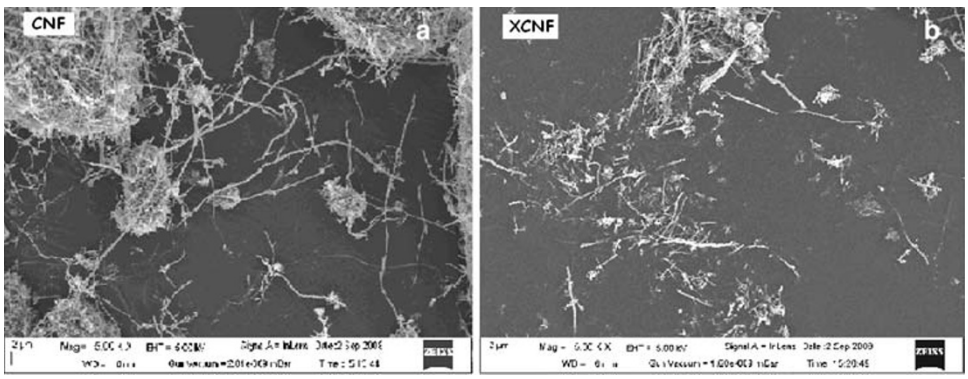

Fig. 3 SEM micrographs of **a** untreated and **b** acid-treated CNFs

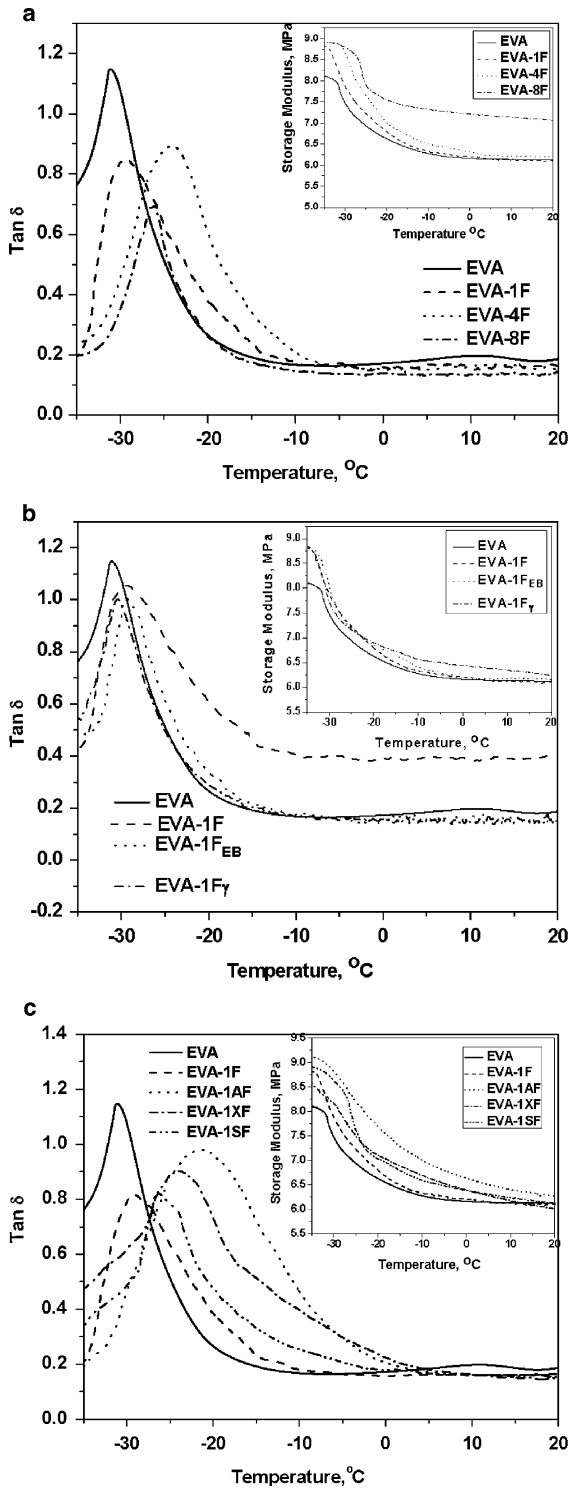

Fig. 4 **a** Tan δ versus temperature and storage modulus versus temperature (*inset*) plots of nanocomposites with different filler loadings. **b** Tan δ versus temperature and storage modulus versus temperature (*inset*) plots of EB irradiated CNF-filled nanocomposites. **c** Tan δ versus temperature and storage modulus versus temperature (*inset*) plots of gamma-irradiated CNF-filled nanocomposites

when 1 wt.% untreated CNF was added to the neat EVA (Table 3). A further increment in the CNF loading to 4 wt.%, enhances the storage modulus by 15% over that of the neat elastomer at the same temperature. The storage modulus of EVA-8F is 16% greater than that of unfilled EVA, at 20 °C.

The glass transition temperature (T_g) for EVA occurs at −30.8 °C and there is a marginal shift of 2.4 °C in T_g toward higher temperature (Table 3) for EVA-1F. A significant shift of 6.6 °C is observed for the nanocomposite with 4 wt.% untreated CNF. For the composite with 8 wt.% CNF loading, the T_g is shifted toward lower temperature region (~2 °C from that of 4 wt.% CNF-filled sample), showing that at higher loadings filler–filler interactions start dominating the filler–polymer interactions. The tan δ peak heights of all the nanocomposites are lower than that of the neat EVA film, which confirms the increase in filler–polymer interaction. When molecular mobility is restricted due to the presence of reinforcing fibers, it results in not only enhanced glass transition temperature, but also in decreased tan δ peak magnitude. The loss modulus versus temperature plots of the nanocomposites with varying filler loadings provide a similar trend (data not shown here). The glass transition temperature appears at still lower temperature. There is only single T_g of the nanocomposites and there is no separate transition for confined EVA chains as effected by CNF.

Thus, the optimum enhancement in the glass transition for EVA-1AF indicates that there exists a significant restriction on the segmental mobility of these polymer chains, which in turn suggests that the polymer chains are in close proximity and interact significantly with the nanofibers and this is further confirmed from the solvent swelling studies.

Swelling Studies

Table 4 reports the volume fraction of rubber (V_r) in each of the cured nanocomposite samples along with that of the virgin EVA elastomer. V_r is considered as a measure of the crosslink density of the sample which in turn represents the extent of interaction developed between the reinforcement and the matrix. The higher the V_r, the higher will be the polymer–filler interaction. It can be observed from the table that as the CNF content increases up to 4 wt.%, the value of V_r increases and then shows a decrease at higher loading. This is in agreement with the results obtained from the results of mechanical and dynamic mechanical properties. Both high-energy as well as chemically modified (except acid treated) CNF-reinforced composites exhibit increased V_r values, indicating increased interaction due to the presence of polar groups and defect sites on the nanofiber surface.

Table 3 Dynamic mechanical analysis data of various nanocomposites

Sample	T_g (°C)	Storage modulus (MPa)		Tan δ	
		T_g	20 °C	T_g	20 °C
EVA	−30.8	7.68	6.10	1.09	0.22
EVA-1F	−29.4	7.38	6.13	0.85	0.17
EVA-4F	−24.2	7.56	6.20	0.89	0.16
EVA-8F	−26.4	8.38	7.07	0.69	0.14
EVA-1F$_{EB}$	−29.4	7.86	6.17	0.85	0.17
EVA-1F$_{\gamma}$	−30.4	7.87	6.24	0.85	0.17
EVA-1AF	−21.5	7.84	6.28	0.98	0.16
EVA-1XF	−27.2	7.79	6.09	0.92	0.15
EVA-1SF	−25.9	7.92	6.15	0.93	0.16

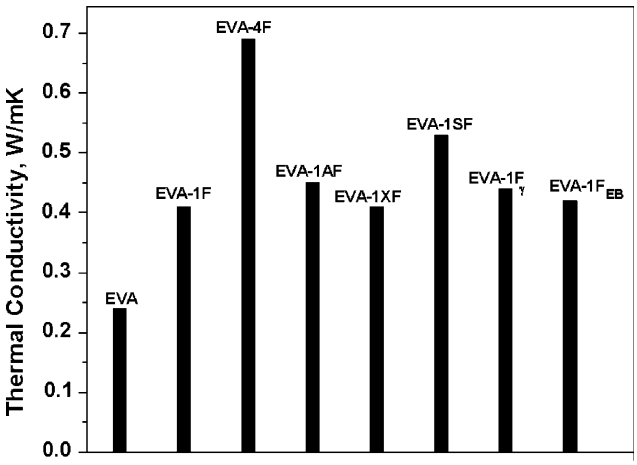

Fig. 5 Thermal conductivity of various nanocomposites

Thermal Conductivity

CNFs have a superior intrinsic thermal conductivity of about 2000 W/mK. However, there is difficulty in translating this intrinsic property in to a strong composite property due to the large number of interfaces that any thermal signal must cross. Addition of CNFs significantly improves the thermal conductivity of EVA even at low loading (Fig. 5).

The thermal conductivity shows an increment of 70 and 188% with incorporation of 1 and 4 wt.% of CNFs, respectively. All the modified CNFs except acid treated one give rise to improved thermal conductivity for the nanocomposites, as compared to untreated CNF-filled sample. The samples EVA-1F$_{EB}$ and EVA-1F$_{\gamma}$ exhibit increments of 2 and 7%, respectively, over that of EVA-1F, whereas EVA-1AF and EVA-1SF show improvements of 10 and 29%, respectively. These enhancements are attributed to the better dispersion and interaction of the nanofibers within the rubber matrix after modification.

Table 4 Volume fraction of rubber in the swollen polymer mass (V_r) of various samples

Sample	Volume fraction of rubber (V_r)
EVA	0.11
EVA-1F	0.17
EVA-4F	0.28
EVA-8F	0.24
EVA-1F$_{EB}$	0.19
EVA-1F$_{\gamma}$	0.20
EVA-1AF	0.19
EVA-1XF	0.14
EVA-1SF	0.20

Thermal Degradation Studies of Nanocomposites

The thermal decomposition behavior of all the nanocomposites is shown in Fig. 6. The CNF-filled nanocomposites display higher thermal stability compared with virgin EVA. The maximum rates of degradation and corresponding temperatures for various nanocomposites are reported in Table 5. The temperature of maximum rate of degradation, T_{Max}, is marginally shifted by 3 and 8 °C for EVA-1F and EVA-4F, respectively. This might have resulted from the good interaction between EVA and CNFs and can be explained by the restrictions on the mobility of the macromolecules imposed by the CNFs. Since these fibers have nanodimensions, they impose a vast number of restriction sites, causing a reduction in tension induced by thermal excitation in the carbon–carbon bond. Consequently, the

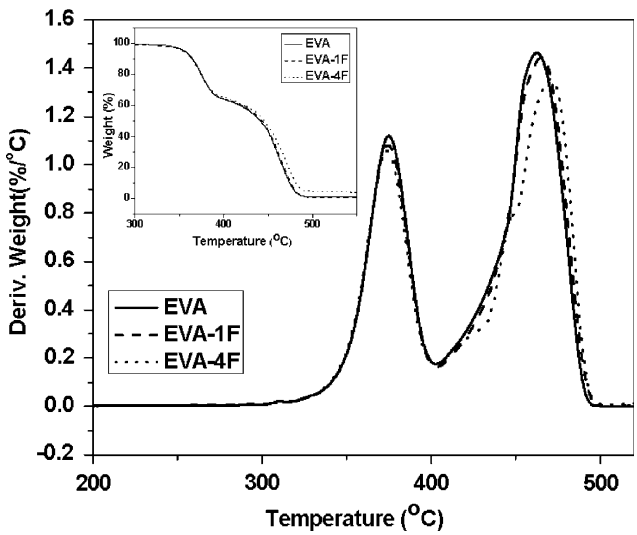

Fig. 6 TGA and DTG plots of various nanocomposites

Table 5 Thermal degradation data of various nanocomposites

Sample	Temperature at which maximum degradation occurs (°C)	Maximum rate of degradation (°C/min)
EVA	462	1.46
EVA-1F	465	1.45
EVA-4F	470	1.35
EVA-1F$_{EB}$	465	1.46
EVA-1F$_{\gamma}$	465	1.43
EVA-1AF	465	1.44
EVA-1XF	459	1.50
EVA-1SF	466	1.43

thermal stability of the polymer increases significantly. However, various modified CNF-reinforced composites do not show any significant improvement in thermal stability at 1 wt.% loading when compared to the untreated CNF-filled ones. EVA-1XF reduces T_{Max} because of the reasons described earlier.

Conclusions

Introduction of a small amount of CNFs can lead to improved performance of EVA. At 4 wt.% CNF loading, the modulus and the tensile strength of the nanocomposite increased substantially. However, similar improvements were not observed at higher (8 wt.%) nanofiller loading due to filler agglomeration. Surface treatment of CNFs with high-energy irradiations of EB and gamma irradiation resulted in improved fiber to matrix interaction, which was supported by swelling resistance studies. This in turn enhanced the dispersion and wetting properties of the nanofibers leading to further improvements in mechanical, dynamic mechanical, and thermal properties of the nanocomposites. At similar loading of filler (1 wt.%), EVA-1SF and EVA-1F$_{\gamma}$ exhibited the best overall properties. The morphological studies revealed that the modified CNFs were better dispersed and distributed in the elastomer matrix at low loadings.

Acknowledgment The authors acknowledge the financial assistance provided by DRDO, New Delhi, India.

References

1. http://www.apsci.com. Accessed 12 December 2007
2. G.G. Tibbetts, M.L. Lake, K.L. Strong, B.P. Rice, Compos. Sci. Technol. **1709**, 67 (2007)
3. P. He, Y. Gao, J. Lian, L. Wang, D. Qian, J. Zhao, W. Wang, M.J. Schulz, X.P. Zhou, D. Shi, Composites Part A **1270**, 37 (2006)
4. T. Prasse, J.Y. Cavaille, W. Bauhofer, Compos. Sci. Technol. **1835**, 63 (2003)
5. Y.K. Choi, K. Sugimoto, S.M. Song, Y. Gotoh, Y. Ohkoshi, M. Endo, Carbon **43**(10), 2199 (2005)
6. W. Brandl, G. Marginean, V. Chirila, W. Warschewski, Carbon **5**, 42 (2004)
7. M.C. Galetz, T. Bla, H. Ruckdaschel, J.K.W. Sandler, V. Altstadt, U. Glatzel. J. Appl. Polym. Sci. **4173**, 104 (2007)
8. K. Lozano, S. Yang, R.E. Jones, Carbon **2329**, 42 (2004)
9. S. Kumar, H. Doshi, M. Srinivasarao, J.O. Park, D.A. Schiraldi, Polymer **1701**, 43 (2002)
10. J. Zeng, B. Saltysiak, W.S. Johnson, D.A. Schiraldi, S. Kumar, Composites Part B **173**, 35 (2004)
11. J. Sandler, A.H.W. Indle, P. Werner, V. Altstadt, M.V. Es, M.S.P. Shaffer, J. Mater. Sci. **2135**, 38 (2003)
12. Y. Yang, M.C. Gupta, K.L. Dudley, R.W. Lawrence, Nanotechnology **1545**, 15 (2004)
13. S. Yang, R. Benitez, A. Fuentes, K. Lozano, Compos. Sci. Technol. **1159**, 67 (2007)
14. E. Hammel, X. Tang, M. Trampert, T. Schmitt, K. Mauthner, A. Eder, P. Potschke, Carbon **1153**, 42 (2004)
15. R.L. Jacobsen, D.G. Glasgow, in *Proceedings of the American Society for Composites, 14th Technical Conference* (Applied Sciences, Inc., Cedarville, OH, 1999), p. 987
16. A. Michael, K. Hilmar, T. Barney, A. Max, V. Richard, Polym. Prepr. (Am. Chem. Soc. Div. Polym. Chem.) **47**(1), 476 (2006)
17. Y. Yang, M.C. Gupta, K.L. Dudley, R.W. Lawrence, Nanotechnology **1545**, 15 (2004)
18. C. Gauthier, L. Chazeau, T. Prasse, J.Y. Cavaille, Compos. Sci. Technol. **335**, 65 (2005)
19. P. Richard, T. Prasse, J.Y. Cavaille, L. Chazeau, C. Gauthier, J. Duchet, Mater. Sci. Eng. A **344**, 352 (2003)
20. Y. Gao, P. He, J. Lian, M.J. Schulz, J. Zhao, W. Wang, X. Wang, J. Zhang, X. Zhou, D. Shi, J. Appl. Polym. Sci. **103**(6), 3792 (2007)
21. J.J. George, A. Bandyopadhyay, A.K. Bhowmick, J. Appl. Polym. Sci. **108**(3), 1603 (2008). doi:10.1002/app.25067
22. J.J. George, R. Sengupta, A.K. Bhowmick, J. Nanosci. Nanotechnol. **8**(4), 1913 (2008)